Z. Angew. Math. Phys. (2016) 67:53
© 2016 Springer International Publishing
0044-2275/16/030001-19
published online April 29, 2016
DOI 10.1007/s00033-016-0650-2

Zeitschrift für angewandte Mathematik und Physik ZAMP

Three-dimensional instabilities of pantographic sheets with parabolic lattices: numerical investigations

Daria Scerrato, Ivan Giorgio and Nicola Luigi Rizzi

Abstract. In this paper, we determine numerically a large class of equilibrium configurations of an elastic two-dimensional continuous pantographic sheet in three-dimensional deformation consisting of two families of fibers which are parabolic prior to deformation. The fibers are assumed (1) to be continuously distributed over the sample, (2) to be endowed of bending and torsional stiffnesses, and (3) tied together at their points of intersection to avoid relative slipping by means of internal (elastic) pivots. This last condition characterizes the system as a pantographic lattice (Alibert and Della Corte in Zeitschrift für angewandte Mathematik und Physik 66(5):2855–2870, 2015; Alibert et al. in Math Mech Solids 8(1):51–73, 2003; dell'Isola et al. in Int J Non-Linear Mech 80:200–208, 2016; Int J Solids Struct 81:1–12, 2016). The model that we employ here, developed by Steigmann and dell'Isola (Acta Mech Sin 31(3):373–382, 2015) and first investigated in Giorgio et al. (Comptes rendus Mecanique 2016, doi:10.1016/j.crme.2016.02.009), is applicable to fiber lattices in which three-dimensional bending, twisting, and stretching are significant as well as a resistance to shear distortion, i.e., to the angle change between the fibers. Some relevant numerical examples are exhibited in order to highlight the main features of the model adopted: In particular, buckling and post-buckling behaviors of pantographic parabolic lattices are investigated. The fabric of the metamaterial presented in this paper has been conceived to resist more effectively in the extensional bias tests by storing more elastic bending energy and less energy in the deformation of elastic pivots: A comparison with a fabric constituted by beams which are straight in the reference configuration shows that the proposed concept is promising.

Mathematics Subject Classification. 74A30 · 74B20 · 74S05.

Keywords. Nonlinear elasticity, Second gradient models, Woven fabrics.

1. Introduction

Design and synthesis of new materials that satisfy some required specific characteristics is a very attractive challenge that researchers have tackled since many years in different branches of physics as electromagnetism, optics, or mechanics. Those assumptions which usually are accepted to be valid while modeling "natural" materials lead to useful simplifications on which many engineering applications have been based up to now. In particular, two-dimensional and three-dimensional continuum models have been formulated based on so-called Cauchy assumptions, which lead to the classical definition of stress and strain states. However, and based on purely logical considerations, already Gabrio Piola (see [33,39]) clearly proved that not all conceivable materials can be modeled under the simplifying assumptions put forward by Cauchy, Poisson, and Navier (for a discussion of this point, see, e.g., [33,40] and references there quoted).

1.1. Higher gradient continuum models for metamaterials

Already Piola considered the possibility to include in the deformation energy of three-dimensional continua together with the first gradient of placement also its second and possibly higher gradients, and he bases his argument on the eventual need to include in these models the description of long range interaction between the material particles. Piola's point of view has been recovered, many years later, for instance, by Mindlin and Toupin [73,111]. When dealing with two-dimensional continua, the classical models due to Love and Kirchhoff do include higher gradient of transverse displacements as independent variables in the constitutive equation for deformation energy but, when considering tangential displacements, they restrict the attention to the particular case of dependence on first gradient of aforementioned tangential displacements. In the more recent papers [3–5,45] and [41,55,107–109], this last restriction is removed and so-called geodesic bending is taken into account for the determination of deformation energy. The more general models thus formulated allow for the theoretical framing of more sophisticated models which are able to describe the behavior of a large class of metamaterials, as those considered in the present paper.

Indeed, when fabrics are constituted at microlevel by highly inhomogeneous materials and are formed by microscopically complex geometric patterns, then the modeling assumptions accepted after Cauchy must be generalized if macroscopic homogenized models need to be introduced (see, e.g., [40]). More and more often, such fabrics are attracting the attention of the researchers in material sciences: Indeed, so-called tailored or architectured or optimized or smart materials are more and more often being conceived and studied because of their specific and unconventional behavior (for more details on this subject, see, e.g., [17,31,38] and the references there cited).

The word *metamaterials* is a neologism which was constructed from the Greek word *meta-*, (meaning *to go beyond*) composed with the Latin root *materia*. Metamaterials are materials designed and engineered in order to have properties which have not yet been observed in nature, which go beyond those materials which are already known. One has to remark, however, that if a property was not observed yet in nature may simply mean that nobody looked for it, due to the lack of suitable theoretical tools of investigation and modeling and that with a careful search, one can find even natural materials having such an exotic property.

It seems to us that, in the context of Mechanical Sciences, this new concept focused on the design and synthesis of new materials, rather than on the analysis of common materials already employed, is quite little exploited when compared with what is done in the other fields of physics already mentioned.

It also seems to us that the introduction of higher gradient models may be of help in the investigation and design of a large class of metamaterials, although we are aware of the fact that more generally microstructured continua [50,51] may be necessary: In this context, the results presented in [1,2,104] prove rigorously that for a particular class of microfabrics, the macro-models must be second gradient continua. The controversy about the relevance of higher gradient continua seems to have been solved by several results proving that many systems showing microscopic complexity can be modeled, at a suitably large scale, by higher gradient continua (see, e.g., [1,12,17,24,43,44,57,65,84,93]). Actually, an exhaustive review on the conceptual bases of higher gradient continuum theories may be found in [40] while interesting applications are found in [28,87,88,94,102,116,117]. Remark also that nonlinear higher gradient elasticity is necessary also when the correct frame for continua having energetic boundaries is looked for (see, e.g., [67]).

1.2. Range of applicability for generalized continuum models

In technological applications, many and different microfabrics are considered to form microarchitectured metamaterials. The different mechanical parts constituting these fabrics may be fibers, microbeams, microplates, or any other kinds of structural element. All considered structural elements may be constrained by suitable elastic or perfect constraints, and their mechanical properties may be extremely different from each other. A possible way for assembling fibers could be to weave them: In this case, the constraint is obtained by means of friction forces whose effectiveness may depend on the state of stress at the contact interface between different fibers. In this case, a particular attention must be paid to frictional slip (as done, for instance, in [75]) while other peculiar properties of several kinds of composite materials [66,77,78,103] have also been taken into account.

In the literature, many different generalized continuum models have been proposed for mechanical systems including inextensible and extensible fibers: see, e.g., [35,37,55,107,109] and references there cited. To our knowledge, however, it has not been addressed yet the problem of studying the deformation of second gradient plates having two families of extensible material curves having nonvanishing referential curvature and being capable of storing deformation energy when their curvature is changing. Some relevant results in the formulation of the needed theories can be found in [46–48] where local symmetry properties for elastic generalized shells are studied and in [3–5,45] where some theories of plates and shells with microstructure are presented. Remark that the problems addressed in the present paper are static. A dynamical analysis of second gradient plates needs to be developed, and for the first results in this context presented the reader is referred, e.g., to [34,36,52,106]. Besides, considering that the system under study is very light, applications in which there is a fluid–structure interaction could show an unexpected behavior which seems worthy of study (see, e.g., [13,76,79,80,82] for more details on this issue). It has also to be remarked that nonstandard and exotic dynamical behavior can be described in some particular micromorphic continua [91] and in multi-physics metamaterials, as those conceived to exploit piezoelectric transduction see, e.g., [29,81,92,98] and the references there cited.

Finally, it has to be remarked that microscopically complex systems are not designed by engineers only: Indeed, nature, and in particular evolution, produced many tissues whose microscopic fabric is very complex: Some efforts are being directed toward the formulation of generalized continuum models in this context: Some relevant works are [11,49,54,58,63,64,69,90,102,110].

The presented method features also the possibility of describing buckling and post-buckling phenomena, as in its deformation energy some nonquadratic terms depending on some deformation energies are introduced. The buckling and post-buckling analysis performed here is purely numerical: We are aware of the fact that only via suitable analytical or semi-analytical studies (those presented in [6,53,85,86,95–97,101], [14,71,72] and [26,27,115] seem to us relevant in our context), it will become possible a complete classification of such behaviors.

1.3. Experimental and numerical characterization of higher gradient constitutive parameters

In order to use the introduced second gradient model to get effective predictions of considered metamaterials (as done in [38]), one has to identify macroscopic constitutive parameters in terms of the specific microstructure under consideration. In this paper, we have used for obtaining such identification the semi-analytical results presented in [89]. We are aware that this analysis needs to be improved and generalized. We intend, in future investigations, to use to this aim several numerical and experimental methodologies: The most relevant in this context seem to be, e.g., those presented in [105,112] where the problem of the identification of macro-properties of structures is addressed or those in [42,70] where viscosity effects are introduced in the picture. Remark that pantographic structures considered here include small elements in which a relatively larger amount of deformation energy may be stored: Therefore, experimental non-invasive detection of damage methods based on dynamic features as natural frequency, eigenmodes, may be used (see, e.g., [30]) together with dynamic characterization and vibration absorption methods (see, e.g., [15,16,18,99,100]) or even the more sophisticated impact analysis (see, e.g., [7–10]).

While experimental evidence is the ultimate check for every modeling effort, also in the context of microscopically complex fabrics, it can be useful to get quantitative and qualitative results about their behavior by resorting to micromodels and intensive numerical simulations, based on simpler mechanical models valid at lower length scales. In this context, isogeometric numerical analysis (see, e.g., [21,22,60,62,113]) or other numerical methods (see, e.g., [19,20,23,25,59,61,114]) have been successfully applied to very similar mechanical problems. Remark that recently some alternative methods (see, e.g., [32,68,74]) based on generalized cellular automata calculations have been proposed which seems suitable to describe numerically the time evolution of higher gradient continua.

1.4. Organization of the paper and the main result presented

In this paper, we want to explore the possibility of designing new fabric sheets with a particular arrangement of the fibers to obtain specific and uncommon mechanical features different from the usual woven fabrics in which the fibers are straight lines.

Herein, we focus on the following key idea: to use the fibers having a parabolic form in the reference configuration and resisting to variations in curvature. In this way, we intend to exploit the benefit of the greater resistance given by curved beams to improve the extensional strength of the designed metamaterial. The model used here in order to describe this class of fabrics employs two-dimensional second gradient continuum theory of elastic surfaces to model three-dimensional placements and deformations of fibered pantographic sheets: This model has been recently developed by Steigmann and dell'Isola [108]. The results which we present indicate that the same amount of the same material can be reorganized at microlevel in order to form microstructures whose extensional resistance is nearly one order of magnitude greater.

The paper is organized as follows:

- Section 2 describes the features of the model employed in this paper; more specifically, in Sect. 2.1, the kinematics of the considered 2D continuum is specified, together with its material symmetry class; in Sect. 2.2, the deformation measures are decomposed in order to take into account the material symmetry properties of a parabolic pantographic sheet; in Sect. 2.3, a suitable deformation energy is postulated. All equilibrium configurations will be determined by minimization methods.
- Section 3 shows the most relevant numerical simulations which we have obtained. In particular, we show that (1) the force exerted in extensional bias test (in a suitably chosen optimal direction relative to fiber orientation) in parabolic pantographic sheet is larger than in the case of microstructure formed by straight lines; (2) interesting out-of-plane buckling and post-buckling phenomena may occur beyond suitable thresholds in extension tests; (3) interesting wrinkling out-of-plane shapes are formed in the case of imposed planar shear and compression boundary displacements. The numerical integration scheme must be based on intensive application of Argyris planar finite element, as the space in which the minimization problem for second gradient energies is formed by the set of functions having integrable second-order weak derivatives. This is the reason for which isogeometric methods (applied in very similar contexts in [21,60,62]) seem suitable to supply a very efficient numerical tool.
- Section 4 concludes the paper by indicating the novel properties of considered parabolic pantographic sheets. They include (1) higher extensional resistance in specific directions, (2) relatively low mass/resistance ratio, (3) localized patterns of deformation energy, and (4) capability of producing specific wrinkling out-of-plane patterns.

2. 2D pantographic sheets with initially parabolic fibers

2.1. Kinematics

We consider a plane sheet formed from two families of fibers that initially are curved and lie parallel to the coordinate lines of a two-dimensional orthogonal coordinate system, i.e., confocal parabolas. We treat the sheet as a 2D continuum, so that introducing the parabolic coordinates $\{\varphi, \psi\}$ every line in which φ or ψ are constant in the initial rectangular domain $\mathcal{B}$ is regarded as a fiber. Specifically, in a Cartesian coordinate system $\{X_1, X_2\}$, the fibers are defined by the curves of constant φ

$$2X_2 = \frac{X_1^2}{\varphi^2} - \varphi^2 \tag{1}$$

and the curves of constant ψ

$$2X_2 = -\frac{X_1^2}{\psi^2} + \psi^2 \tag{2}$$

When a deformation occurs, the material particle that initially is at the point $\boldsymbol{X} = (X_1, X_2) \in \mathcal{B}$ goes to the point in 3D space whose place is indicated by the map $\boldsymbol{r}(X_1, X_2) : \mathcal{B} \subset \mathbb{R}^2 \mapsto \mathbb{R}^3$. By introducing the components of displacement u_i along the three unit vectors of the Cartesian coordinate system $\{\mathbf{e}_i\}$, we can express the placement map as

$$\boldsymbol{r}(X_\alpha) = X_\alpha \mathbf{e}_\alpha + u_i(X_\alpha)\mathbf{e}_i \tag{3}$$

with Latin indexes ranging from 1 to 3 and Greek indexes from 1 to 2. The derivatives of $\boldsymbol{r}$ are denoted by

$$\boldsymbol{a}_\alpha = \boldsymbol{r}_{,\alpha} \tag{4}$$

The deformation gradient $\boldsymbol{F} = \nabla \boldsymbol{r}$ thus can be written as

$$\boldsymbol{F} = \boldsymbol{a}_\alpha \otimes \mathbf{e}_\alpha \tag{5}$$

Therefore, the Cauchy–Green deformation tensor is given by

$$\boldsymbol{C} = \boldsymbol{F}^\top \boldsymbol{F} = C_{\alpha\beta}\, \mathbf{e}_\alpha \otimes \mathbf{e}_\beta \tag{6}$$

As a result, the strain tensor $\boldsymbol{E}$, in terms of its components, becomes

$$E_{\alpha\beta} = \frac{1}{2}\left(C_{\alpha\beta} - \delta_{\alpha\beta}\right) \quad \text{with} \quad C_{\alpha\beta} = r_{i,\alpha} r_{i,\beta} \tag{7}$$

with $\delta_{\alpha\beta}$ the Kronecker delta. Here, we consider also the second gradient of the deformation, $\nabla \boldsymbol{F} = \nabla\nabla \boldsymbol{r}$, i.e., the third-order tensor $\nabla \boldsymbol{F} = \boldsymbol{F}_{,\alpha} \otimes \mathbf{e}_\alpha$, in order to describe the fiber curvatures and twist [41,108].

2.2. Fiber decompositions

Let $\{\boldsymbol{L}(\boldsymbol{X}), \boldsymbol{M}(\boldsymbol{X})\}$ be orthogonal families of unit vectors in the plane of $\mathcal{B}$ defining the fiber directions in the reference configuration. Assuming the fibers to be material curves with no relative slipping and tied together at their points of intersection, we can represent the fibers' directions after the deformation with the families of unit vectors $\{\boldsymbol{l}(\boldsymbol{X}), \boldsymbol{m}(\boldsymbol{X})\}$ given by

$$\lambda \boldsymbol{l} = \boldsymbol{F}\boldsymbol{L}, \quad \mu \boldsymbol{m} = \boldsymbol{F}\boldsymbol{M} \tag{8}$$

where λ and μ are the fiber stretches. As a result, we may use $\{\boldsymbol{l}, \boldsymbol{m}\}$ spanning the deformed tangent plane at the material point $\boldsymbol{X}$ to define the fiber shear angle γ by

$$\sin\gamma = \boldsymbol{l} \cdot \boldsymbol{m} \tag{9}$$

For a parabolic net, from Eq. (1), we obtain

$$\varphi^2 = 2\left(\|\boldsymbol{X}\| - X_2\right) \tag{10}$$

choosing the root of Eq. (1) that is always positive, and then, we may evaluate its gradient

$$\nabla\varphi = \frac{1}{\varphi}\left(\frac{\boldsymbol{X}}{\|\boldsymbol{X}\|} - \mathbf{e}_2\right) \tag{11}$$

and, therefore, the vectors $\boldsymbol{L}(\boldsymbol{X})$ and $\boldsymbol{M}(\boldsymbol{X})$ as

$$\boldsymbol{L}(\boldsymbol{X}) = \frac{\nabla\varphi}{\|\nabla\varphi\|} \quad \text{and} \quad \boldsymbol{M}(\boldsymbol{X}) = \mathbf{e}_3 \times \boldsymbol{L}(\boldsymbol{X}) \tag{12}$$

Employing the fiber decomposition proposed in [108], the gradient of deformation may be represented as

$$\boldsymbol{F} = \lambda \boldsymbol{l} \otimes \boldsymbol{L} + \mu \boldsymbol{m} \otimes \boldsymbol{M} \tag{13}$$

and thus, the Cauchy–Green deformation tensor is

$$\boldsymbol{C} = \lambda^2 \boldsymbol{L} \otimes \boldsymbol{L} + \mu^2 \boldsymbol{M} \otimes \boldsymbol{M} + \lambda\mu \sin\gamma \, (\boldsymbol{L} \otimes \boldsymbol{M} + \boldsymbol{M} \otimes \boldsymbol{L}) \tag{14}$$

while the second gradient of the deformation can be written as [108]

$$\nabla\nabla \boldsymbol{r} = (\boldsymbol{g}_l + K_L \boldsymbol{n}) \otimes \boldsymbol{L} \otimes \boldsymbol{L} + (\boldsymbol{g}_m + K_M \boldsymbol{n}) \otimes \boldsymbol{M} \otimes \boldsymbol{M} + (\boldsymbol{\Gamma} + T\boldsymbol{n}) \otimes (\boldsymbol{L} \otimes \boldsymbol{M} + \boldsymbol{M} \otimes \boldsymbol{L}), \tag{15}$$

with

$$\mathbf{g}_l = \lambda^2 \eta_l \, \boldsymbol{p} + (\boldsymbol{L} \cdot \nabla\lambda) \, \boldsymbol{l}, \quad \boldsymbol{g}_m = \mu^2 \eta_m \, \boldsymbol{q} + (\boldsymbol{M} \cdot \nabla\mu) \, \boldsymbol{m} \tag{16}$$

and

$$\boldsymbol{\Gamma} = (\boldsymbol{L} \cdot \nabla\mu) \, \boldsymbol{m} + \lambda\mu\phi_m \, \boldsymbol{q} = (\boldsymbol{M} \cdot \nabla\lambda) \, \boldsymbol{l} + \lambda\mu\phi_l \, \boldsymbol{p}, \tag{17}$$

in which η_l and η_m are the geodesic curvatures of the deformed fibers, ϕ_l and ϕ_m are the so-called Tchebychev curvatures, and

$$\boldsymbol{p} = \boldsymbol{n} \times \boldsymbol{l}, \quad \boldsymbol{q} = \boldsymbol{n} \times \boldsymbol{m} \quad \text{and} \quad \boldsymbol{l} \times \boldsymbol{m} = |\cos\gamma| \boldsymbol{n} \tag{18}$$

define the orthogonal directions of the fibers on the deformed surface, while

$$K_L = \lambda^2 \kappa_l, \quad K_M = \mu^2 \kappa_m \quad \text{and} \quad T = \lambda\mu\tau, \tag{19}$$

where κ_l and κ_m are the normal curvatures of the deformed fibers, and τ measures the twist of the deformed surface. These are nonzeros if the deformation is such as to generate a curvature of the surface in 3D space. Accordingly, they describe those parts of the fiber curvatures that can be attributed to surface flexure, whereas the geodesic curvatures represent the components of fiber curvatures in the tangent planes of the deformed surface.

2.3. Strain energy

In this paper, as done in [56], we postulate the first term of the elastic stored energy as follows:

$$W^I(\varepsilon_L, \varepsilon_M, J) = \frac{1}{2} Y_L \varepsilon_L^2 + \frac{1}{2} Y_M \varepsilon_M^2 - G_{LM} \left[\ln(J) + 1 - J\right] \tag{20}$$

where Y_L, Y_M, and G_{LM} are positive material constants, and suitable strain measures (see, e.g., [56,108]) are employed

$$\begin{aligned} \varepsilon_L &= E_{\alpha\beta} L_\alpha L_\beta = \frac{1}{2}\left(\lambda^2 - 1\right) \\ \varepsilon_M &= E_{\alpha\beta} M_\alpha M_\beta = \frac{1}{2}\left(\mu^2 - 1\right) \\ J &= \| L_\alpha M_\beta \boldsymbol{r}_{,\alpha} \times \boldsymbol{r}_{,\beta} \| = \| \lambda \boldsymbol{l} \times \mu \boldsymbol{m} \| \end{aligned} \tag{21}$$

Indeed, ε_L and ε_M are measures of fiber extension along $\boldsymbol{L}$ and $\boldsymbol{M}$ directions, respectively, and J is the area stretch. The second energy term may be assumed as follows:

$$W^{II} = \tfrac{1}{2}(A_L \, |\boldsymbol{g}_l|^2 + A_M \, |\boldsymbol{g}_m|^2 + A_\Gamma \, |\boldsymbol{\Gamma}|^2 + k_L K_L^2 + k_M K_M^2 + k_T T^2), \tag{22}$$

Therefore, a simple strain energy function incorporating the curvilinear orthotropic symmetry associated with the initial fiber geometry is

$$W = W^I(\varepsilon_L, \varepsilon_M, J) + W^{II}(\boldsymbol{g}_l, \boldsymbol{g}_m, \boldsymbol{\Gamma}, K_L, K_M, T) \tag{23}$$

3. Numerical examples

In this section, we show some numerical examples employing the model sketched above and proposed in [108], adopting a rectangular domain whose edges are in ratio 1:3 and consisting of a parabolic fiber net; in all the cases analyzed, it is assumed that the samples have the same arrangement of the fibers unless otherwise specified. The FE analysis is performed by using COMSOL Multiphysics, a software flexible enough to allow us to insert any kind of nonstandard strain energies not necessarily included in its libraries. Specifically, we utilize Eq. (23) which is characterized by a term depending on the second gradient of displacement. For this reason, we adopt the Argyris element which is an element of class $\mathcal{C}^1$ and thus particularly suitable to approximate the solution of the problem under study.

In what follows, the above formulation is recast in a nondimensional form by normalizing the elastic energy (23) with respect to a reference stiffness while the lengths are normalized with respect to the shorter edge. Nondimensional quantities are denoted by a superimposed tilde.

The constitutive parameters assumed in the current analysis are listed below:

$$\tilde{Y}_L = 100, \quad \tilde{Y}_M = 100, \quad \tilde{G}_{LM} = 0.2,$$
$$\tilde{A}_L = \tilde{k}_L = 0.01, \quad \tilde{A}_M = \tilde{k}_M = 0.01, \quad \tilde{A}_\Gamma = \tilde{k}_T = 0.1 \tag{24}$$

In the first case, we examine the standard bias extension test in which one of the shorter side is fixed, and on the other, a uniform displacement is imposed which is equal to 0.8 and orthogonal to the same side. In particular, Fig. 1 displays the arrangement of the fibers in the reference configuration (Fig. 1a), the equilibrium shape of the sample after the deformation and the new disposition of the net (Fig. 1b), the measure of the shear strain γ (Fig. 1c), and the second gradient energy (Fig. 1d). The plot of γ in Fig. 1c shows the presence of two distinct areas separated by a transition zone because of the presence of

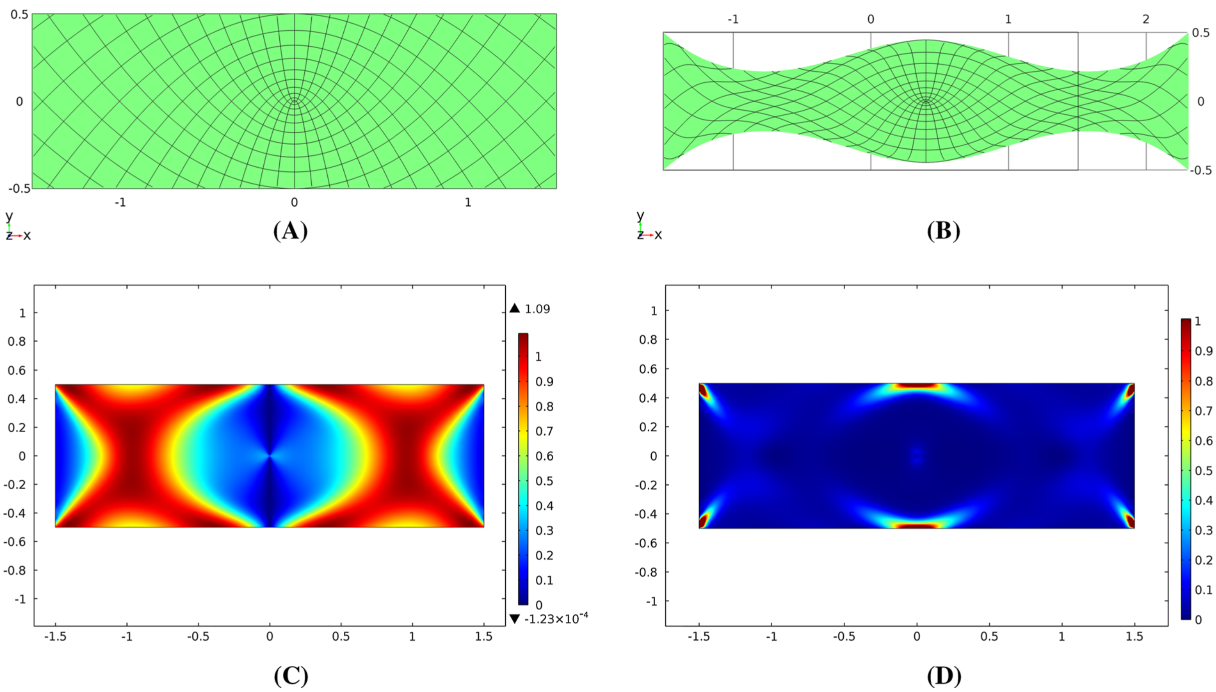

FIG. 1. Bias extension test—case I, **a** reference fiber pattern, **b** actual fiber pattern, **c** fiber shear angle γ, **d** second gradient energy

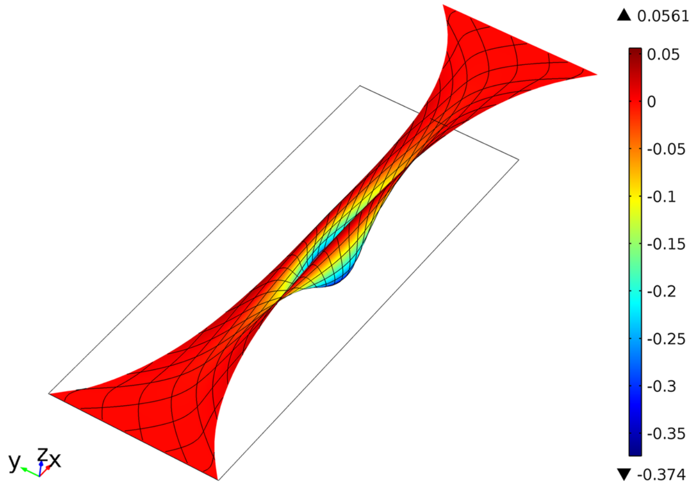

Fig. 2. Bias extension test—case I: buckling shape related to the critical displacement

a second gradient energy term. This behavior is quite standard for a bias extension test of fabric sheets (see, e.g., [56]). However, in the common bias test performed on sheets with straight fibers, three regions characterized by a uniform fiber shear angle can be easily recognized. In our parabolic case, instead only two areas with almost constant shear angle are detected, one with a fiber shear angle γ almost nil and the other with an angle decrease of about 60°. Besides, in Fig. 1d, a localization of a second gradient energy in a narrow region along the largest parabolic fibers inscribed in the sample can be observed.

In the bias test considered, the displacement imposed on the sample under test along the direction of X_1-axis, due to the particular arrangement of the parabolic fibers, induces a compression of the straight fibers parallel to the vector $\mathbf{e}_2$ and therefore a buckling phenomenon occurs in correspondence with a critical displacement. This last mentioned has been evaluated as $\tilde{u}_1 = 0.8984$. Figure 2 displays the buckling mode related to this critical displacement; the colors indicate the out-of-plane component of displacement, $\tilde{u}_3$. To determine an equilibrium shape related to the buckling mode, we take geometrical and mechanical imperfections into account by imposing on short sides the additional boundary condition on the derivatives of the displacement out of plane of the pantographic sheet and, in particular, we set $\tilde{u}_{3,\alpha}\nu_\alpha = 2 \times 10^{-4}$, where $\boldsymbol{\nu}$ is the unit vector normal to the edge and on the plane determined by the vectors $\mathbf{e}_1$ and $\mathbf{e}_2$.

In order to explore the features of the fiber arrangement considered, we compare two kinds of samples: one constituted by a straight and orthogonal lattice of fibers, and the other characterized by a parabolic net as it has been already analyzed. Specifically, we investigate the behavior of these two arrangements in the cases of a bias extension test and a shear displacement imposed.

In the former case, we plot the equilibrium shapes for three imposed displacements along the direction of the X_1-axis, $\tilde{u}_1 = \{0.31, 0.62, 0.85\}$; in Fig. 3, the colors indicate the distribution of the shear angle γ, while in Fig. 4 they are related to the total strain energy density. We can observe that the maximum value of the shear angle γ is almost the same for the two fiber dispositions, but the stored strain energy is much greater in the case of parabolic fibers.

Similar considerations apply in the latter case when one short edge is fixed and a displacement is imposed in the direction of the X_2-axis on the opposite side (see Fig. 5). Finally, for a quantitative comparison, we show the overall constraint reactions by varying the imposed displacement in the two tests under examination (see Fig. 9), and once again, it is confirmed that the arrangement of the parabolic net is much stiffer than the one with straight fibers.

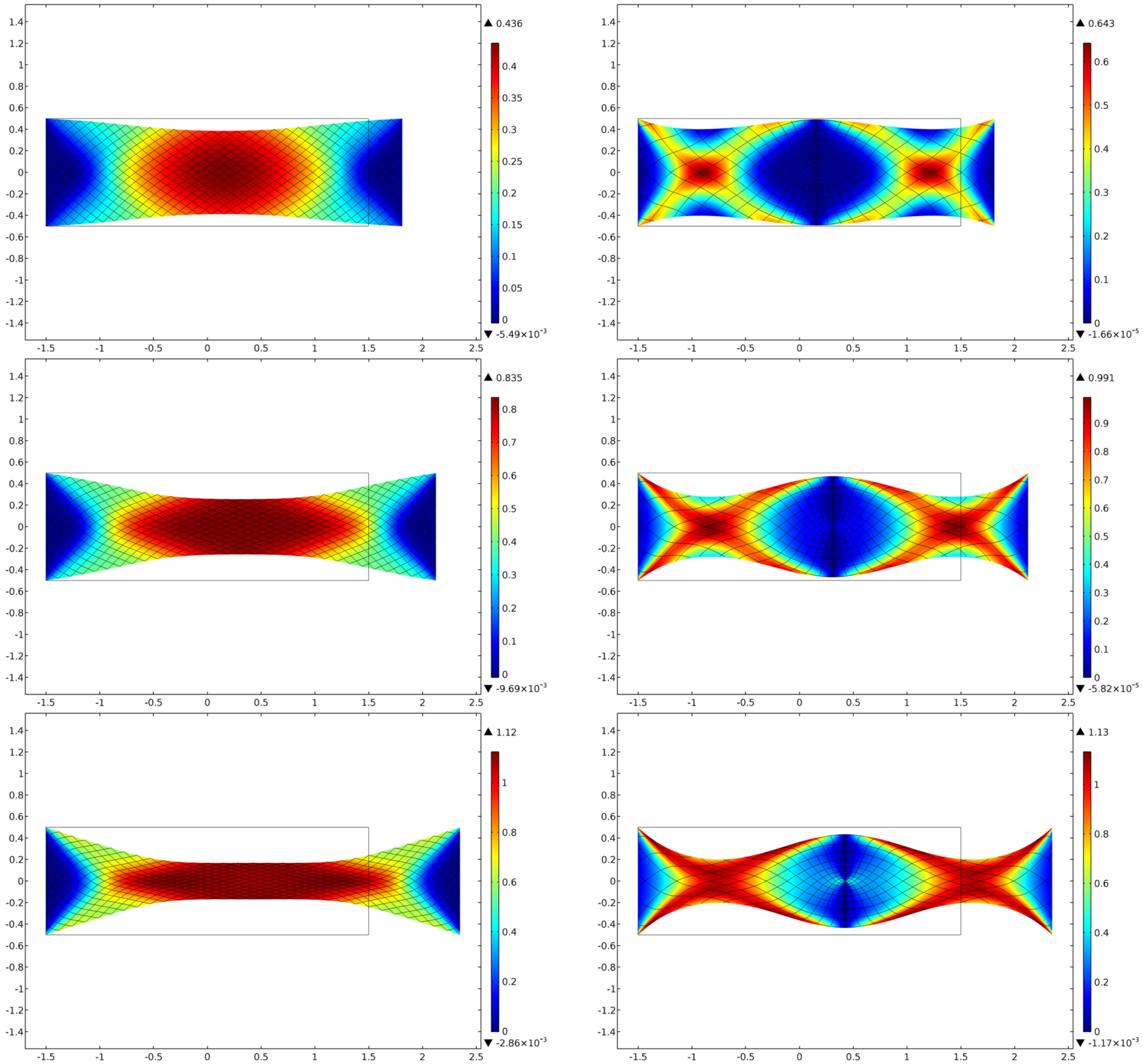

Fig. 3. Comparison between straight and parabolic fibers: bias extensional test with imposed displacement {0.31, 0.62, 0.85}. The *colors* indicate the shear angle γ (color figure online)

Afterward, the standard bias extension test is applied to a specimen with a different initial arrangement of the fibers (see Fig. 6). The considered sheet is deformed by fixing it at one shorter edge and assigning a uniform displacement of amplitude 1 at the opposite boundary so as to move away these two sides. Figure 6 exhibits from left to right the fiber pattern prior to deformation, the equilibrium shape of the sample after the deformation and the new disposition of the net, the measure of the shear strain γ, and the second gradient energy. Similarly, to the previous case, two main zones kept separate from transition regions can be noticed, i.e., one with a fiber shear angle γ close to zero and the other with an angle increase of about 75° (see Fig. 6). This time, it is much more evident that the localization of the second gradient energy occurs along the transition regions.

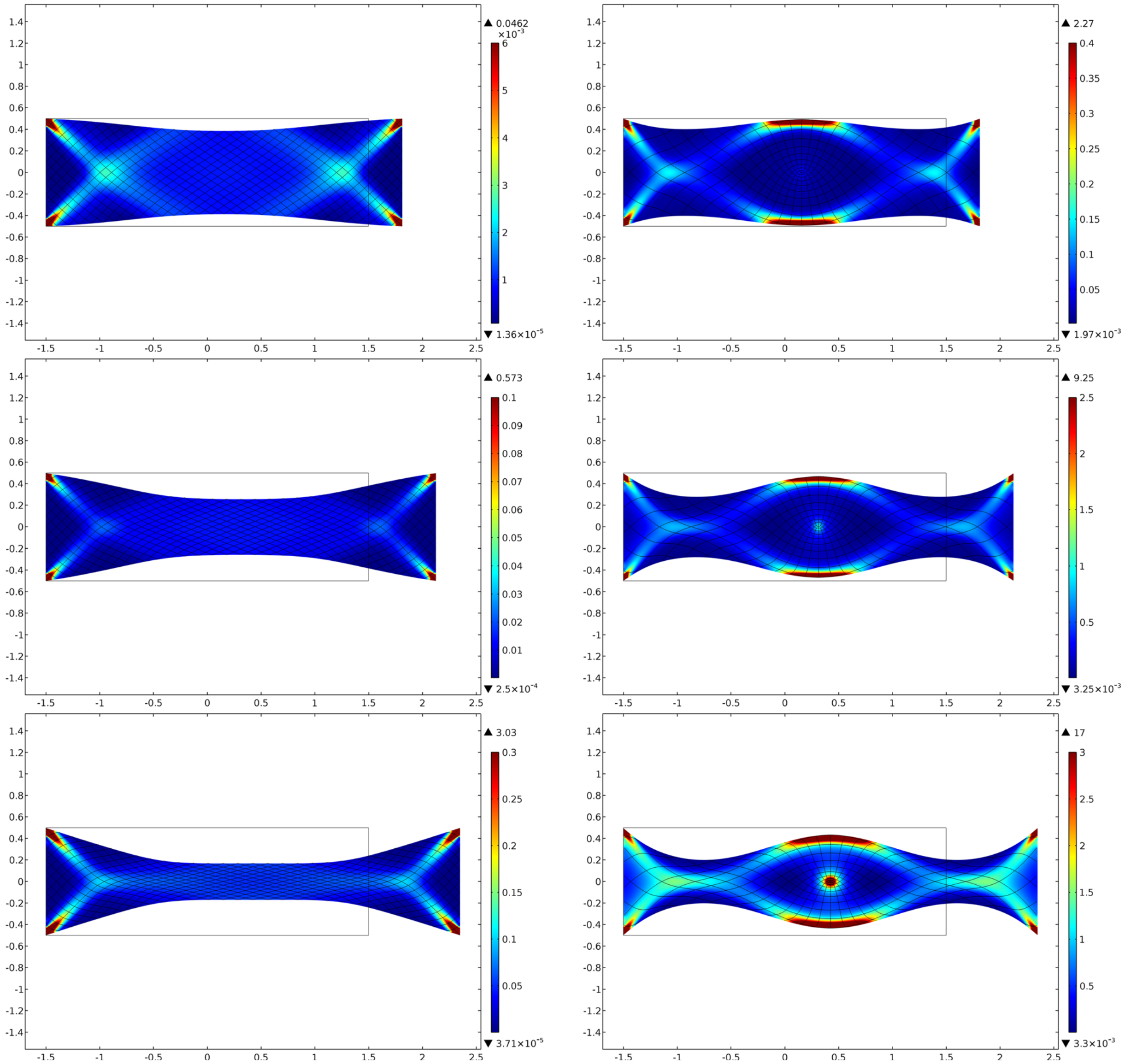

FIG. 4. Comparison between straight and parabolic fibers: bias extensional test with imposed displacement {0.31, 0.62, 0.85}. The *colors* indicate the total strain energy density (color figure online)

In the next example, we impose a relative rotation and translation to the opposite shorter boundaries in order to cause bending, stretching, and twisting in three dimensions. In more detail, we fix one edge and assign the following displacement field on the other edge

$$\begin{cases} \tilde{u}_1 & = 0.3 \\ \tilde{u}_2 & = \left(s - \frac{1}{2}\right)(\cos\vartheta - 1) \\ \tilde{u}_3 & = \left(s - \frac{1}{2}\right)\sin\vartheta \end{cases} \tag{25}$$

where s is a parameter which varies from 0 to 1, and ϑ is a rotation angle with respect to the longitudinal axis of rectangle, here assumed to be equal to $\pi/3$. Figure 7 shows the equilibrium shape (Fig. 7a), where

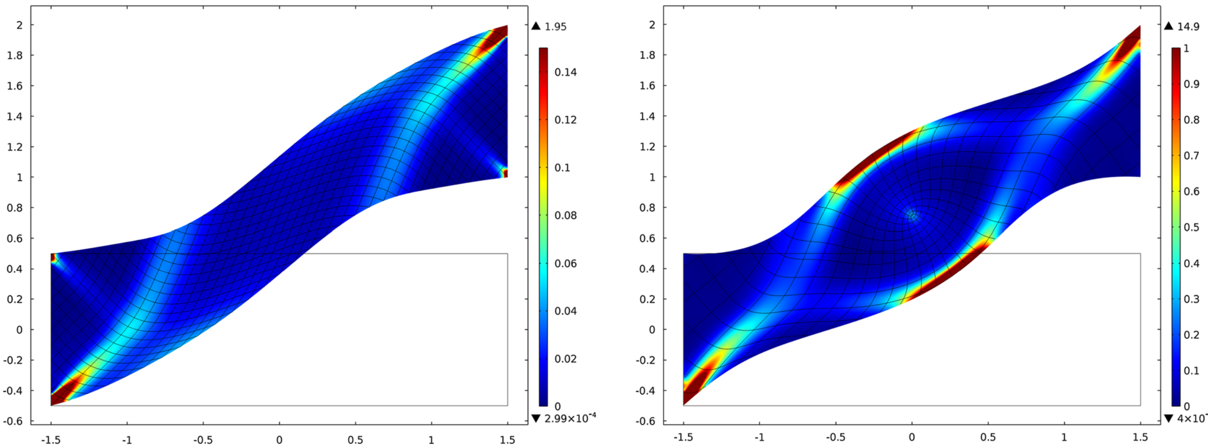

FIG. 5. Test with shear displacement imposed: Equilibrium shapes related to straight fibers (*left*), parabolic fibers (*right*). The *colors* indicate the total strain energy density (color figure online)

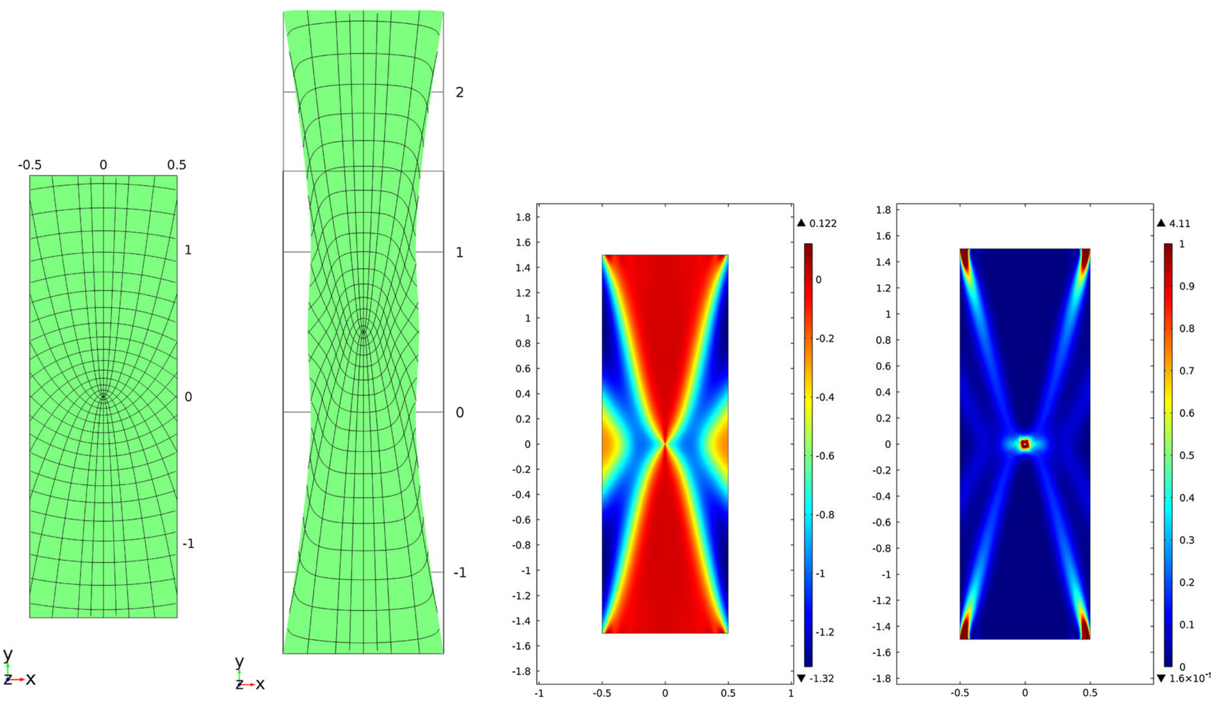

FIG. 6. Bias extension test—case II, in the given order: reference and actual fiber patterns; the fiber shear angle γ; second gradient energy

colors indicate the out-of-plane component of displacement, $\tilde{u}_3$, and the fiber pattern is highlighted; the fiber shear angle γ (Fig. 7b); the first gradient energy (Fig. 7c); and the second gradient energy (Fig. 7d).

Also in this case, we can observe a localization of both energies of first and second gradients near the largest parabolic fibers.

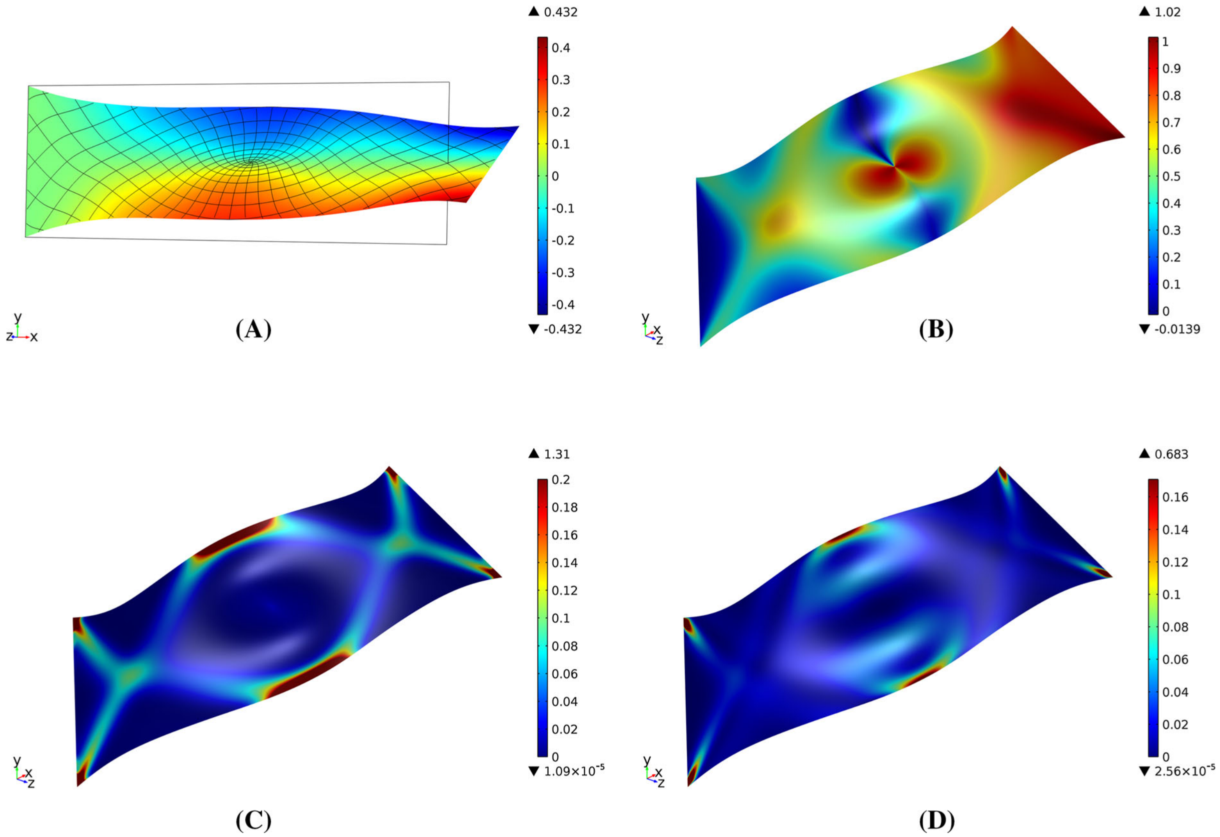

Fig. 7. Test with stretching ($\tilde{u}_1 = 0.3$) and twist ($\vartheta = 60°$), **a** equilibrium shape and fiber pattern, **b** fiber shear angle γ, **c** first gradient energy, **d** second gradient energy

We complete this gallery of examples with a case of buckling in which compressive and shear displacements, respectively, $\tilde{u}_2 = -0.2$ and $\tilde{u}_1 = 0.5$, are imposed on one of the long sides; the opposite edge is fixed, and the short sides are left free. In addition, on the moving long side, we assign the extra-constraint: $\tilde{u}_{3,\beta}\nu_\beta = \left(1 \times 10^{-4}\right) s$, where $\beta = \{1, 2\}$, s is a parameter which varies from 0 to 1, and $\boldsymbol{\nu}$ is the unit vector normal to the edge and on the plane determined by the vectors $\mathbf{e}_1$ and $\mathbf{e}_2$. Figure 8 exhibits the fiber pattern and the equilibrium shape (Fig. 8a), where colors indicate the out-of-plane component of displacement, $\tilde{u}_3$; the fiber shear angle γ (Fig. 8b); the first gradient energy (Fig. 8c); and the second gradient energy (Fig. 8c). It should be noted that at the central area of the sample, a geodesic buckling appears in the plane of the fabric sheet.

4. Conclusions

In modern engineering, there are three features which are more and more frequently demanded to novel materials: (1) the capability to resist in an elastic way in large deformation regimes, (2) the capability to resist to applied load also when damage phenomena start to occur, (3) the capability of localizing deformation energy so that the parts of the system to be checked in order to assess its integrity are determined a priori.

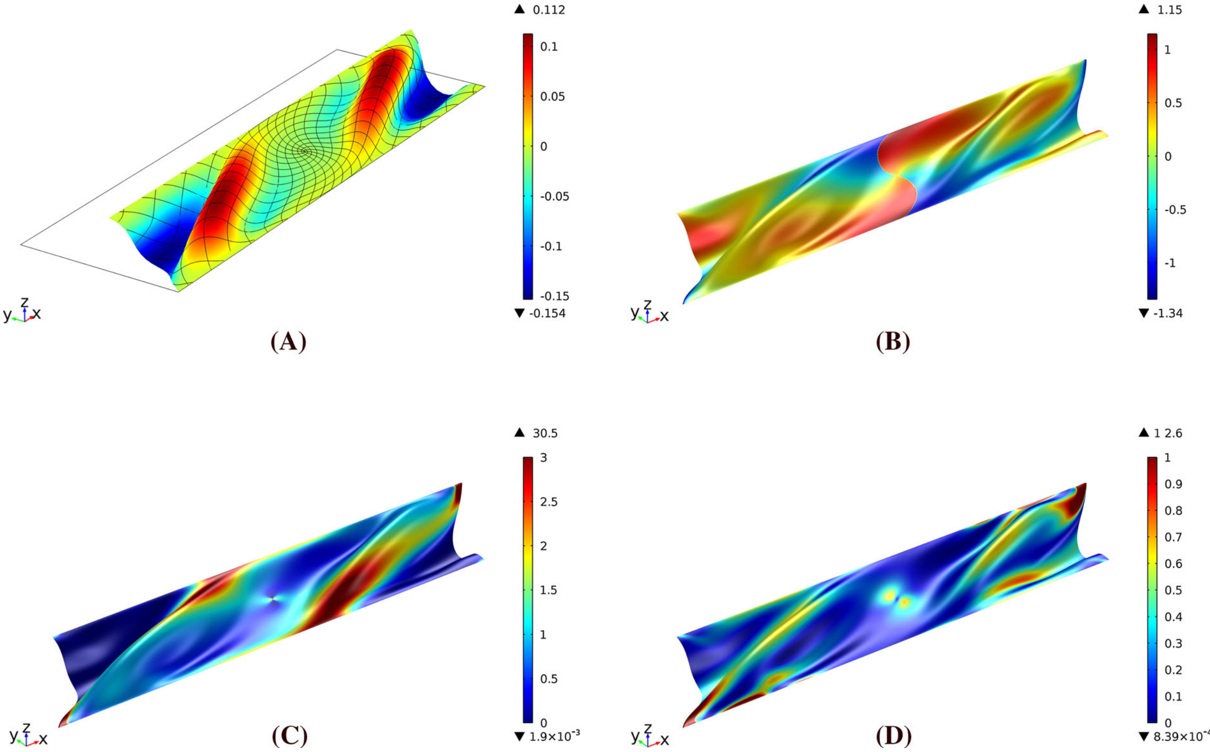

Fig. 8. Example of buckling with shear ($\tilde{u}_1 = 0.5$) and compressive ($\tilde{u}_2 = -0.2$) displacement imposed, **a** equilibrium shape and fiber pattern, **b** fiber shear angle γ, **c** first gradient energy, **d** second gradient energy

In this paper, we try to prove the applicability and feasibility of the following concept: Given a mass of an elastic material, it is possible to arrange it in order to form a network of beams connected by cylinders (playing the role of elastic pivots) to get a fabric which is able to undergo large deformations remaining in elastic regimes and is capable of sustaining externally applied loads even when some damage phenomenon occurs.

The presented analysis did not consider any model for damage onset and evolution: However, we could verify that in the most relevant deformation patterns, the conceived fabric actually shows high concentration of deformation energy: It is therefore likely that damage onset will be localized in these regions. Future investigations will address the relevant related modeling issues.

An aspect of the microstructure introduced here concerns the shape of the involved beams in the stress-free reference configuration: We have assumed it is parabolic. Indeed, we assumed that a parabolic system of coordinates in the reference configuration characterizes the material symmetries of the considered fabric. The enhanced bending deformation of such fibers (when comparing the performances of the present fabric with that constituted by straight lines) produces a greater stiffness in bias extension test without changing the capability of undergoing large deformations in the elastic regime (see Fig. 9).

Indeed, to use interconnected fibers having a parabolic form in the reference configuration allows us to exploit the benefit of the greater resistance to deformation given by pre-curved beams. The designed metamaterial results to have an improved extensional strength.

The model used here in order to describe parabolic pantographic sheets is based on the second gradient continuum theory of elastic surfaces which can undergo three-dimensional large placements and deformations recently developed by Steigmann and dell'Isola [108].

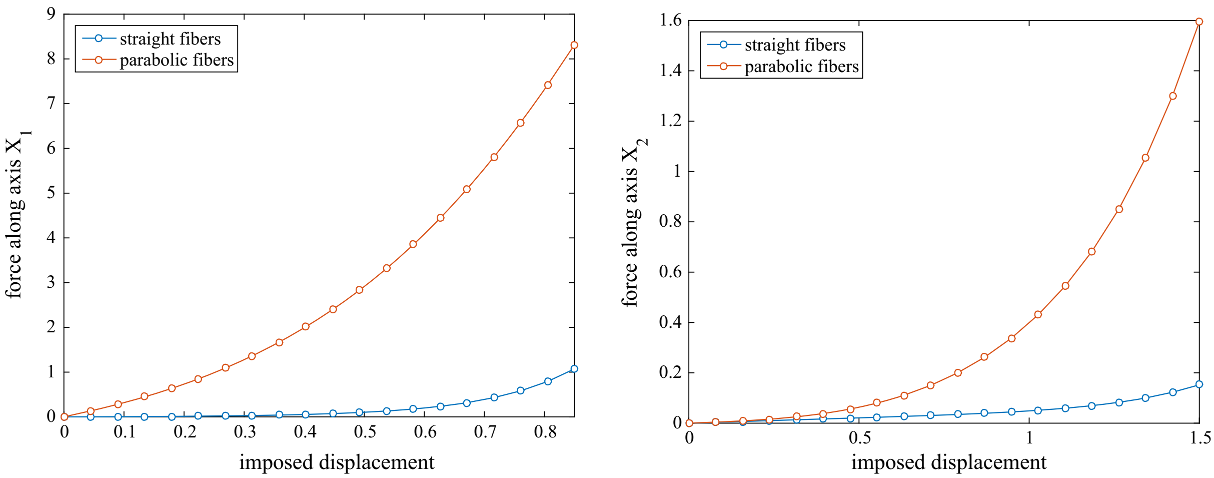

FIG. 9. Comparison between parabolic and straight fibers: bias extensional test (*left*), test with shear displacement imposed (*right*)

As a by-product of performed numerical simulations, we prove that many wrinkling shapes of considered pantographic sheets are assumed in equilibrium conditions even when purely plane boundary displacements are imposed. These buckling phenomena are expected but not yet described in the literature together with their post-buckling evolution. We intend to systematically investigate these phenomena by means of the perturbative methods described in [83].

A more difficult problem consists in looking for optimized microstructures which are able to perform some assigned tasks: We claim that it can be of use the introduction of generalized continuum models in this kind of investigations.

Acknowledgements

The authors thank Professors David Steigmann and Francesco dell'Isola for helpful comments and advice through the study.

References

1. Alibert, J.-J., Della Corte, A.: Second-gradient continua as homogenized limit of pantographic microstructured plates: a rigorous proof. Zeitschrift für Angewandte Mathematik Und Physik **66**(5), 2855–2870 (2015)
2. Alibert, J.-J., Seppecher, P., dell'Isola, F.: Truss modular beams with deformation energy depending on higher displacement gradients. Math. Mech. Solids **8**(1), 51–73 (2003)
3. Altenbach, H., Eremeyev, V.A.: On the linear theory of micropolar plates. ZAMM-Zeitschrift für Angewandte Mathematik Und Mechanik **89**(4), 242–256 (2009)
4. Altenbach, H., Eremeyev, V.A.: On the shell theory on the nanoscale with surface stresses. Int. J. Eng. Sci. **49**(12), 1294–1301 (2011)
5. Altenbach, J., Altenbach, H., Eremeyev, V.A.: On generalized Cosserat-type theories of plates and shells: a short review and bibliography. Arch. Appl. Mech. **80**(1), 73–92 (2010)
6. AminPour, H., Rizzi, N.: A one-dimensional continuum with microstructure for single-wall carbon nanotubes bifurcation analysis. Math. Mech. Solids **21**(2), 168–181 (2016)
7. Andreaus, U., Baragatti, P., Placidi, L.: Experimental and numerical investigations of the responses of a cantilever beam possibly contacting a deformable and dissipative obstacle under harmonic excitation. Int. J. Non-Linear Mech. **80**, 96–106 (2016). doi:10.1016/j.ijnonlinmec.2015.10.007

8. Andreaus, U., Casini, P.: Dynamics of SDOF oscillators with hysteretic motion-limiting stop. Nonlinear Dyn. **22**(2), 145–164 (2000)
9. Andreaus, U., Casini, P.: Friction oscillator excited by moving base and colliding with a rigid or deformable obstacle. Int. J. Non-Linear Mech. **37**(1), 117–133 (2002)
10. Andreaus, U., Chiaia, B., Placidi, L.: Soft-impact dynamics of deformable bodies. Contin. Mech. Thermodyn. **25**(2–4), 375–398 (2013)
11. Andreaus, U., Giorgio, I., Lekszycki, T.: A 2-D continuum model of a mixture of bone tissue and bio-resorbable material for simulating mass density redistribution under load slowly variable in time. ZAMM-Zeitschrift für Angewandte Mathematik Und Mechanik **94**(12), 978–1000 (2014)
12. Camar-Eddine, M., Seppecher, P.: Determination of the closure of the set of elasticity functionals. Arch. Ration. Mech. Anal. **170**(3), 211–245 (2003)
13. Carassale, L., Freda, A., Marrè-Brunenghi, M.: Effects of free-stream turbulence and corner shape on the galloping instability of square cylinders. J. Wind Eng. Ind. Aerodyn. **123**, 274–280 (2013)
14. Carassale, L., Piccardo, G.: Non-linear discrete models for the stochastic analysis of cables in turbulent wind. Int. J. Non-Linear Mech. **45**(3), 219–231 (2010)
15. Carcaterra, A., Akay, A., Bernardini, C.: Trapping of vibration energy into a set of resonators: theory and application to aerospace structures. Mech. Syst. Signal Process. **26**, 1–14 (2012)
16. Carcaterra, A., D'Ambrogio, W.: An iterative rational fraction polynomial technique for modal identification. Meccanica **30**(1), 63–75 (1995)
17. Carcaterra, A. dell'Isola, F., Esposito, R., Pulvirenti, M.: Macroscopic description of microscopically strongly inhomogenous systems: a mathematical basis for the synthesis of higher gradients metamaterials. Arch. Ration. Mech. Anal. **218**(3), 1239–1262 (2015). doi:10.1007/s00205-015-0879-5
18. Carcaterra, A., Roveri, N.: Tire grip identification based on strain information: theory and simulations. Mech. Syst. Signal Process. **41**(1), 564–580 (2013)
19. Cazzani, A., Garusi, E., Tralli, A., Atluri, S.N.: A four-node hybrid assumed-strain finite element for laminated composite plates. CMC Comput. Mater. Continua **2**(1), 23–38 (2005)
20. Cazzani, A., Lovadina, C.: On some mixed finite element methods for plane membrane problems. Comput. Mech. **20**(6), 560–572 (1997)
21. Cazzani, A., Malagù, M., Turco, E.: Isogeometric analysis of plane-curved beams. Math. Mech. Solids. doi:10.1177/1081286514531265 (2014)
22. Cazzani, A., Malagù, M., Turco, E., Stochino, F.: Constitutive models for strongly curved beams in the frame of isogeometric analysis. Math. Mech. Solids. **21**(2), 182–209 (2016). doi:10.1177/1081286515577043
23. Cazzani, A., Ruge, P.: Numerical aspects of coupling strongly frequency-dependent soil-foundation models with structural finite elements in the time-domain. Soil Dyn. Earthq. Eng. **37**, 56–72 (2012)
24. Cecchi, A., Rizzi, N.L.: Heterogeneous elastic solids: a mixed homogenization-rigidification technique. Int. J. Solids Struct. **38**(1), 29–36 (2001)
25. Cesarano, C., Cennamo, G.M., Placidi, L.: Humbert polynomials and functions in terms of Hermite polynomials towards applications to wave propagation. WSEAS Trans. Math. **13**, 595–602 (2014)
26. Challamel, N., Lerbet, J., Wang, C.M., Zhang, Z.: Analytical length scale calibration of nonlocal continuum from a microstructured buckling model. ZAMM-Zeitschrift für Angewandte Mathematik Und Mechanik **94**(5), 402–413 (2014)
27. Challamel, N., Zhang, Z., Wang, C.M.: Nonlocal equivalent continua for buckling and vibration analyses of microstructured beams. J. Nanomech. Micromech. **5**, A4014004-1–A4014004-16 (2014). doi:10.1061/(ASCE)NM.2153-5477.0000062
28. Chiaia, B., Kumpyak, O., Placidi, L., Maksimov, V.: Experimental analysis and modeling of two-way reinforced concrete slabs over different kinds of yielding supports under short-term dynamic loading. Eng. Struct. **96**, 88–99 (2015)
29. D'Annibale, F., Rosi, G., Luongo, A.: Linear stability of piezoelectric-controlled discrete mechanical systems under nonconservative positional forces. Meccanica **50**(3), 825–839 (2015)
30. Del Vescovo, D., Fregolent, A.: Theoretical and experimental dynamic analysis aimed at the improvement of an acoustic method for fresco detachment diagnosis. Mech. Syst. Signal Process. **23**(7), 2312–2319 (2009)
31. Del Vescovo, D., Giorgio, I.: Dynamic problems for metamaterials: review of existing models and ideas for further research. Int. J. Eng. Sci. **80**, 153–172 (2014)
32. Della Corte, A., Battista, A., dell'Isola, F.: Referential description of the evolution of a 2D swarm of robots interacting with the closer neighbors: perspectives of continuum modeling via higher gradient continua. Int. J. Non-Linear Mech. **80**, 209–220 (2016). doi:10.1016/j.ijnonlinmec.2015.06.016
33. dell'Isola, F., Andreaus, U., Placidi, L.: At the origins and in the vanguard of peridynamics, non-local and higher-gradient continuum mechanics: an underestimated and still topical contribution of Gabrio Piola. Math. Mech. Solids **20**(8), 887–928 (2015)

34. dell'Isola, F., Della Corte, A., Giorgio, I., Scerrato, D.: Pantographic 2D sheets: discussion of some numerical investigations and potential applications. Int. J. Non-Linear Mech. **80**, 200–208 (2016). doi:10.1016/j.ijnonlinmec.2015.10.010
35. dell'Isola, F., Della Corte, A., Greco, L., Luongo, A.: Plane bias extension test for a continuum with two inextensible families of fibers: a variational treatment with Lagrange Multipliers and a perturbation solution. Int. J. Solids Struct. **81**, 1–12 (2016). doi:10.1016/j.ijsolstr.2015.08.029
36. dell'Isola, F., Giorgio, I., Andreaus, U.: Elastic pantographic 2D lattices: a numerical analysis on static response and wave propagation. Proc. Estonian Acad. Sci. **64**(3), 219–225 (2015)
37. dell'Isola, F., Giorgio, I., Pawlikowski, M., Rizzi, N.L.: Large deformations of planar extensible beams and pantographic lattices: heuristic homogenisation, experimental and numerical examples of equilibrium. Proc. R. Soc. Lond. A **472**, 20150790 (2016). doi:10.1098/rspa.2015.0790
38. dell'Isola, F., Lekszycki, T., Pawlikowski, M., Grygoruk, R., Greco, L.: Designing a light fabric metamaterial being highly macroscopically tough under directional extension: first experimental evidence. Zeitschrift für angewandte Mathematik und Physik. **66**(6), 3473–3498 (2015). doi:10.1007/s00033-015-0556-4
39. dell'Isola, F., Maier, G., Perego, U., Andreaus, U., Esposito, R., Forest, S.: The complete works of Gabrio Piola: volume I—commented english translation. Adv. Struct. Mater. doi:10.1007/978-3-319-00263-7 (2014)
40. dell'Isola, F., Seppecher, P., Della Corte, A.: The postulations á la D'Alembert and á la Cauchy for higher gradient continuum theories are equivalent: a review of existing results. Proc. R. Soc. Lond. A **471**(2183), 20150415 (2015)
41. dell'Isola, F., Steigmann, D.: A two-dimensional gradient-elasticity theory for woven fabrics. J. Elast. **118**(1), 113–125 (2015)
42. Dietrich, L., Lekszycki, T., Turski, K.: Problems of identification of mechanical characteristics of viscoelastic composites. Acta Mech. **126**(1–4), 153–167 (1998)
43. Dos Reis, F., Ganghoffer, J.F.: Construction of micropolar continua from the asymptotic homogenization of beam lattices. Comput. Struct. **112**, 354–363 (2012)
44. Dos Reis, F., Ganghoffer, J.F.: Homogenized elastoplastic response of repetitive 2D lattice truss materials. Comput. Mater. Sci. **84**, 145–155 (2014)
45. Eremeyev, V.A., Altenbach, H., Morozov, N.F.: The influence of surface tension on the effective stiffness of nanosize plates. Doklady Phys. **54**(2), 98–100 (2009)
46. Eremeyev, V.A., Pietraszkiewicz, W.: Local symmetry group in the general theory of elastic shells. J. Elast. **85**(2), 125–152 (2006)
47. Eremeyev, V.A., Pietraszkiewicz, W.: Material symmetry group of the non-linear polar-elastic continuum. Int. J. Solids Struct. **49**(14), 1993–2005 (2012)
48. Eremeyev, V.A., Pietraszkiewicz, W.: Material symmetry group and constitutive equations of micropolar anisotropic elastic solids. Math. Mech. Solids. **21**(2), 210–221 (2016). doi:10.1177/1081286515582862
49. Federico, S., Grillo, A.: Elasticity and permeability of porous fibre-reinforced materials under large deformations. Mech. Mater. **44**, 58–71 (2012)
50. Forest, S.: Micromorphic approach for gradient elasticity, viscoplasticity, and damage. J. Eng. Mech. **135**(3), 117–131 (2009)
51. Forest, S., Sievert, R.: Nonlinear microstrain theories. Int. J. Solids Struct. **43**(24), 7224–7245 (2006)
52. Frischmuth, K., Kosiéski, W., Lekszycki, T.: Free vibrations of finite-memory material beams. Int. J. Eng. Sci. **31**(3), 385–395 (1993)
53. Gabriele, S., Rizzi, N., Varano, V.: On the imperfection sensitivity of thin-walled frames. In: Topping, B.H.V. (ed.) Proceedings of the Eleventh International Conference on Computational Structures Technology. Civil-Comp Press, Stirlingshire, paper 15 (2012). doi:10.4203/ccp.99.15
54. Giorgio, I., Andreaus, U., Lekszycki, T., Della Corte, A.: The influence of different geometries of matrix/scaffold on the remodeling process of a bone and bioresorbable material mixture with voids. Math. Mech. Solids. doi:10.1177/1081286515616052 (2015)
55. Giorgio, I., Della Corte, A., dell'Isola, F., Steigmann, D.J.: Buckling modes in pantographic lattices. Comptes rendus Mecanique (2016). doi:10.1016/j.crme.2016.02.009
56. Giorgio, I., Grygoruk, R., dell'Isola, F., Steigmann, D.J.: Pattern formation in the three-dimensional deformations of fibered sheets. Mech. Res. Commun. **69**, 164–171 (2015)
57. Goda, I., Assidi, M., Ganghoffer, J.-F.: Equivalent mechanical properties of textile monolayers from discrete asymptotic homogenization. J. Mech. Phys. Solids **61**(12), 2537–2565 (2013)
58. Goda, I., Assidi, M., Ganghoffer, J.F.: A 3D elastic micropolar model of vertebral trabecular bone from lattice homogenization of the bone microstructure. Biomech. Model. Mechanobiol. **13**(1), 53–83 (2014)
59. Greco, L., Cuomo, M.: On the force density method for slack cable nets. Int. J. Solids Struct. **49**(13), 1526–1540 (2012)
60. Greco, L., Cuomo, M.: An implicit G1 multi patch B-spline interpolation for Kirchhoff-Love space rod. Comput. Methods Appl. Mech. Eng. **269**, 173–197 (2014)

61. Greco, L., Cuomo, M.: Consistent tangent operator for an exact Kirchhoff rod model. Contin. Mech. Thermodyn. **27**(4), 861–877 (2015)
62. Greco, L., Cuomo, M.: An isogeometric implicit G1 mixed finite element for Kirchhoff space rods. Comput. Methods Appl. Mech. Eng. **298**, 325–349 (2016)
63. Grillo, A., Federico, S., Wittum, G.: Growth, mass transfer, and remodeling in fiber-reinforced, multi-constituent materials. Int. J. Non-Linear Mech. **47**(2), 388–401 (2012)
64. Grillo, A., Wittum, G., Tomic, A., Federico, S.: Remodelling in statistically oriented fibre-reinforced materials and biological tissues. Math. Mech. Solids **20**(9), 1107–1129 (2015)
65. Hans, S., Boutin, C.: Dynamics of discrete framed structures: a unified homogenized description. J. Mech. Mater. Struct. **3**(9), 1709–1739 (2008)
66. Harrison, P.: Modelling the forming mechanics of engineering fabrics using a mutually constrained pantographic beam and membrane mesh. Compos. Part A Appl. Sci. Manuf. **81**, 145–157 (2016)
67. Javili, A., dell'Isola, F., Steinmann, P.: Geometrically nonlinear higher-gradient elasticity with energetic boundaries. J. Mech. Phys. Solids **61**(12), 2381–2401 (2013)
68. Koh, S.J.A., Lee, H.P., Lu, C., Cheng, Q.H.: Molecular dynamics simulation of a solid platinum nanowire under uniaxial tensile strain: temperature and strain-rate effects. Phys. Rev. B **72**(8), 085414 (2005)
69. Lekszycki, T., dell'Isola, F.: A mixture model with evolving mass densities for describing synthesis and resorption phenomena in bones reconstructed with bio-resorbable materials. Zeitschrift für Angewandte Mathematik Und Mechanik **92**(6), 426–444 (2012)
70. Lekszycki, T., Olhoff, N., Pedersen, J.J.: Modelling and identification of viscoelastic properties of vibrating sandwich beams. Compos. Struct. **22**(1), 15–31 (1992)
71. Luongo, A.: Mode localization in dynamics and buckling of linear imperfect continuous structures. In: Vakakis, A.F. (ed.) Normal Modes and Localization in Nonlinear Systems, pp. 133–156. Springer, Berlin (2001)
72. Luongo, A., Zulli, D., Piccardo, G.: On the effect of twist angle on nonlinear galloping of suspended cables. Comput. Struct. **87**(15), 1003–1014 (2009)
73. Mindlin, R.D.: Second gradient of strain and surface-tension in linear elasticity. Int. J. Solids Struct. **1**(4), 417–438 (1965)
74. Misra, A., Roberts, L.A., Levorson, S.M.: Reliability analysis of drilled shaft behavior using finite difference method and Monte Carlo simulation. Geotech. Geol. Eng. **25**(1), 65–77 (2007)
75. Nadler, B., Steigmann, D.J.: A model for frictional slip in woven fabrics. Comptes Rendus Mecanique **331**(12), 797–804 (2003)
76. Nguyen, C.H., Freda, A., Solari, G., Tubino, F.: Aeroelastic instability and wind-excited response of complex lighting poles and antenna masts. Eng. Struct. **85**, 264–276 (2015)
77. Nikopour, H., Selvadurai, A.P.S.: Torsion of a layered composite strip. Compos. Struct. **95**, 1–4 (2013)
78. Nikopour, H., Selvadurai, A.P.S.: Concentrated loading of a fibre-reinforced composite plate: experimental and computational modeling of boundary fixity. Compos. Part B Eng. **60**, 297–305 (2014)
79. Pagnini, L.: Reliability analysis of wind-excited structures. J. Wind Eng. Ind. Aerodyn. **98**(1), 1–9 (2010)
80. Pagnini, L.C.: Model reliability and propagation of frequency and damping uncertainties in the dynamic along-wind response of structures. J. Wind Eng. Ind. Aerodyn. **59**(2), 211–231 (1996)
81. Pagnini, L.C., Piccardo, G.: The three-hinged arch as an example of piezomechanic passive controlled structure. Contin. Mech. Thermodyn. doi:10.1007/s00161-015-0474-x (2015)
82. Pagnini, L.C., Solari, G.: Serviceability criteria for wind-induced acceleration and damping uncertainties. J. Wind Eng. Ind. Aerodyn. **74**, 1067–1078 (1998)
83. Piccardo, G., D'Annibale, F., Zulli, D.: On the contribution of Angelo Luongo to Mechanics: in honor of his 60th birthday. Contin. Mech. Thermodyn. **27**(4), 507–529 (2015)
84. Pideri, C., Seppecher, P.: A second gradient material resulting from the homogenization of an heterogeneous linear elastic medium. Contin. Mech. Thermodyn. **9**(5), 241–257 (1997)
85. Pignataro, M., Rizzi, N., Ruta, G., Varano, V.: The effects of warping constraints on the buckling of thin-walled structures. J. Mech. Mater. Struct. **4**(10), 1711–1727 (2009)
86. Pignataro, M., Ruta, G., Rizzi, N., Varano, V.: Effects of warping constraints and lateral restraint on the buckling of thin-walled frames. ASME Int. Mech. Eng. Congress Exposit. Proc. **10**(PART B), 803–810 (2010)
87. Placidi, L.: A variational approach for a nonlinear one-dimensional damage-elasto-plastic second-gradient continuum model. Contin. Mech. Thermodyn. **28**(1), 119–137 (2016). doi:10.1007/s00161-014-0405-2
88. Placidi, L.: A variational approach for a nonlinear 1-dimensional second gradient continuum damage model. Contin. Mech. Thermodyn. **27**(4), 623–638 (2015)
89. Placidi, L., Andreaus, U., Della Corte, A., Lekszycki, T.: Gedanken experiments for the determination of two-dimensional linear second gradient elasticity coefficients. Zeitschrift für Angewandte Mathematik Und Physik **66**(6), 3699–3725 (2015)

90. Placidi, L., Faria, S.H., Hutter, K.: On the role of grain growth, recrystallization and polygonization in a continuum theory for anisotropic ice sheets. Ann. Glaciol. **39**(1), 49–52 (2004)
91. Placidi, L., Giorgio, I., Della Corte, A., Scerrato, D.: Euromech 563 Cisterna di Latina 17–21, (March 2014) Generalized continua and their applications to the design of composites and metamaterials: a review of presentations and discussions. Math. Mech. Solids. doi:10.1177/1081286515576948 (2015)
92. Porfiri, M., Frattale Mascioli, F.M., dell'Isola, F.: Circuit analog of a beam and its application to multimodal vibration damping, using piezoelectric transducers. Int. J. Circ. Theory Appl. **32**(4), 167–198 (2004)
93. Rahali, Y., Giorgio, I., Ganghoffer, J.F., dell'Isola, F.: Homogenization à la Piola produces second gradient continuum models for linear pantographic lattices. Int. J. Eng. Sci. **97**, 148–172 (2015)
94. Rinaldi, A., Placidi, L.: A microscale second gradient approximation of the damage parameter of quasi-brittle heterogeneous lattices. ZAMM-Zeitschrift für Angewandte Mathematik Und Mechanik **94**(10), 862–877 (2014)
95. Rizzi, N.L., Varano, V.: The effects of warping on the postbuckling behaviour of thin-walled structures. Thin Walled Struct. **49**(9), 1091–1097 (2011)
96. Rizzi, N.L., Varano, V.: On the Postbuckling Analysis of Thin-Walled Frames. Civil-Comp Press, Stirling (2011)
97. Rizzi, N.L., Varano, V., Gabriele, S.: Initial postbuckling behavior of thin-walled frames under mode interaction. Thin Walled Struct. **68**, 124–134 (2013)
98. Rosi, G., Pouget, J., dell'Isola, F.: Control of sound radiation and transmission by a piezoelectric plate with an optimized resistive electrode. Eur. J. Mech. A/Solids **29**(5), 859–870 (2010)
99. Roveri, N., Carcaterra, A.: Damage detection in structures under traveling loads by Hilbert-Huang transform. Mech. Syst. Signal Process. **28**, 128–144 (2012)
100. Roveri, N., Carcaterra, A., Akay, A.: Vibration absorption using non-dissipative complex attachments with impacts and parametric stiffness. J. Acoust. Soc. Am. **126**(5), 2306–2314 (2009)
101. Ruta, G.C., Varano, V., Pignataro, M., Rizzi, N.L.: A beam model for the flexural-torsional buckling of thin-walled members with some applications. Thin Wall. Struct. **46**(7–9), 816–822 (2008)
102. Seddik, H., Greve, R., Zwinger, T., Placidi, L.: A full Stokes ice flow model for the vicinity of Dome Fuji, Antarctica, with induced anisotropy and fabric evolution. The Cryosphere **5**(2), 495–508 (2011)
103. Selvadurai, A.P.S., Nikopour, H.: Transverse elasticity of a unidirectionally reinforced composite with an irregular fibre arrangement: experiments, theory and computations. Compos. Struct. **94**(6), 1973–1981 (2012)
104. Seppecher, P., Alibert, J.-J., dell'Isola, F.: Linear elastic trusses leading to continua with exotic mechanical interactions. J. Phys. Conf. Ser. **319**(1), 012018 (2011)
105. Solari, G., Pagnini, L.C., Piccardo, G.: A numerical algorithm for the aerodynamic identification of structures. J. Wind Eng. Ind. Aerodyn. **69**, 719–730 (1997)
106. Soubestre, J., Boutin, C.: Non-local dynamic behavior of linear fiber reinforced materials. Mech. Mater. **55**, 16–32 (2012)
107. Steigmann, D.J.: Theory of elastic solids reinforced with fibers resistant to extension, flexure and twist. Int. J. Non-Linear Mech. **47**(7), 734–742 (2012)
108. Steigmann, D.J., dell'Isola, F.: Mechanical response of fabric sheets to three-dimensional bending, twisting, and stretching. Acta Mech. Sin. **31**(3), 373–382 (2015)
109. Steigmann, D.J., Pipkin, A.C.: Equilibrium of elastic nets. Philos. Trans. R. Soc. Lond. A Math. Phys. Eng. Sci. **335**(1639), 419–454 (1991)
110. Tomic, A., Grillo, A., Federico, S.: Poroelastic materials reinforced by statistically oriented fibres—numerical implementation and application to articular cartilage. IMA J. Appl. Math. **79**, 1027–1059 (2014)
111. Toupin, R.A.: Theories of elasticity with couple-stress. Arch. Ration. Mech. Anal. **17**(2), 85–112 (1964)
112. Turco, E.: Is the statistical approach suitable for identifying actions on structures?. Comput. Struct. **83**(25), 2112–2120 (2005)
113. Turco, E., Aristodemo, M.: A three-dimensional B-spline boundary element. Comput. Methods Appl. Mech. Eng. **155**(1), 119–128 (1998)
114. Turco, E., Caracciolo, P.: Elasto-plastic analysis of Kirchhoff plates by high simplicity finite elements. Comput. Methods Appl. Mech. Eng. **190**(5), 691–706 (2000)
115. Wang, C.M., Zhang, H., Gao, R.P., Duan, W.H., Challamel, N.: Hencky bar-chain model for buckling and vibration of beams with elastic end restraints. Int. J. Struct. Stabil. Dyn. **15**, 1540007-1–1540007-16 (2015). doi:10.1142/S0219455415400076
116. Yang, Y., Ching, W.Y., Misra, A.: Higher-order continuum theory applied to fracture simulation of nanoscale intergranular glassy film. J. Nanomech. Micromechan. **1**(2), 60–71 (2011)
117. Yang, Y., Misra, A.: Higher-order stress–strain theory for damage modeling implemented in an element-free Galerkin formulation. Comput. Model. Eng. Sci. (CMES) **64**(1), 1–36 (2010)

Daria Scerrato and Ivan Giorgio and Nicola Luigi Rizzi
International Research Center for the Mathematics and Mechanics of Complex Systems - MeMoCS
Università dell'Aquila
Cisterna di Latina, Italy

Ivan Giorgio
Department of Structural and Geotechnical Engineering
Università di Roma La Sapienza
Rome, Italy
e-mail: ivan.giorgio@uniroma1.it

Nicola Luigi Rizzi
Department of Architecture
Università degli studi Roma Tre
Rome, Italy

(Received: February 9, 2016)